

# Interlayer-mediated catalyst engineering for ultra-high aspect ratio silicon nanostructures

Bryan P.J. Benz<sup>\*1,2</sup>, Marco Stampanoni<sup>2,3</sup>, and Lucia Romano<sup>2,3</sup>

<sup>1</sup>Department of Physics and Swiss Nanoscience Institute, University of Basel, 4056 Basel, Switzerland

<sup>2</sup>PSI Center for Photon Science, Paul Scherrer Institut, 5232 Villigen PSI, Switzerland

<sup>3</sup>Institute for Biomedical Engineering, University and ETH Zürich, 8092 Zürich, Switzerland

\*Email: bryan.benz@psi.ch

## Abstract

Reliable and precise etching of silicon nanostructures with ultra-high aspect ratios is required in many fields. Metal assisted chemical etching (MacEtch) in vapor is a plasma-free etching method that attracts considerable attention owing to the ability to create smooth, high aspect ratio nanostructures. MacEtch understanding and applications are limited by low fidelity and inconsistent pattern transfer from the catalyst layer to the silicon substrate. The locally constrained electrochemical interactions at the catalyst site make MacEtch particularly sensitive to catalyst contamination reducing the reaction rate and pinning the catalyst during etching. Removing contaminants is essential to improve pattern transfer for reliable processes on a larger area and higher aspect ratio. Physically separating the main source of carbon - the resist - from the catalyst with a sacrificial and functional interlayer solves this issue. The interlayer separates the resist and the catalyst and allows for thorough cleaning of the substrate before catalyst deposition. The resulting clean catalyst has improved stability, quality and reproducibility, enabling reliable fabrication of dense (50% patterned area) high aspect ratio ( $>250:1$ ) nanostructures. Two different interlayer materials (Cr and  $\text{Al}_2\text{O}_3$ ) and two patterning approaches are presented, showcasing etching of various high aspect ratio nanostructures, such as X-ray Optics.

## Introduction

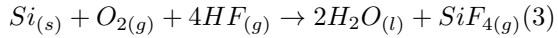
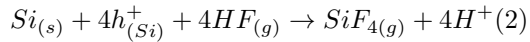
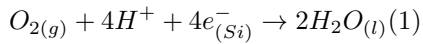
The micro- and nanoscale domains benefit significantly from structures with high aspect ratio (HAR) and precise feature control in semiconductor materials. Consequently, etching methods [1] play a crucial technological role in the device miniaturization roadmap and have attracted considerable attention in the nanofabrication era. Metal assisted chemical etching (MacEtch) [2–4] emerged as an alternative technique to conventional methods, with unique advantages of plasma-free and anisotropic nature. MacEtch can etch materials with high anisotropy, smooth sidewalls, and a large range of feature sizes, from 1 nanometer to 100s of micrometers. [5, 6] The associated research encompasses a wide range of applications, including anti-reflective surfaces, [3] photovoltaics, [7] energy harvesting and storage, [8] sensors, [9] bio-interfaces, [10] fingerprints [11], vias [12] and X-ray Optics. [13] The substrates available for

etching via MacEtch are diverse, and include Ge, GaAs, GaN, InP, and predominantly Si. [2] The MacEtch process involves a local electrochemical reaction occurring at the catalyst site. During etching of a silicon substrate, the catalyst sinks into the substrate. The anisotropic nature of etching originates because it occurs predominantly at the interface of the silicon in contact with the catalyst layer. [14] For precise HAR pattern transfer, the catalyst should remain intact during the process. Etch speed differences might appear as a consequence of local pinning of the catalyst tearing the catalyst apart and leading to uncontrolled etching. [15] Under these conditions, MacEtch does not retain the original pattern and instead produces random micro-porosity in the Si substrate. This poses a critical challenge for the consistent manufacturing of nanostructures with vertical sidewalls with respect to the substrate and high fidelity of pattern transfer, such as in semiconductor

electronic chips, photonic devices, and especially in medical applications. Reproducibility and pattern integrity remain the main challenges for MacEtch preventing so far its widespread application in various fields. [16, 17] The patterning approach presented in this work addresses the issue of uncontrolled catalyst movement during MacEtch for dense HAR structures in the sub-micrometer regime in the presence of lithographic processes. The improved patterning demonstrates the relevance of controlled catalyst preparation and unlocks new capabilities of MacEtch in the gas phase for semiconductor manufacturing and X-ray Optics.

## MacEtch in gas phase

MacEtch with reactants and by-products in the gas phase [13, 18] has the advantage of eliminating the step of drying the etched nanostructures after the etching in liquid etchant solutions. [19] In essence, MacEtch in the gas phase is analogous to its liquid counterpart: [20] an oxidant, either  $O_2$  as presented here or  $O_3$ , [21] is reduced at the catalyst side by extracting electrons from Si or equivalently injecting positive charge carriers in the underlying substrate, causing the oxidation of silicon; [22] the etchant, hydrofluoric-acid (HF), attacks oxidized silicon, leading to Si removal at the interface with the catalyst, with the consequent sinking of the catalyst into the substrate. In gas, the oxidant of choice is  $O_2$  and the catalyst is Pt. Other options are available, but this combination achieves the best pattern transfer for MacEtch in the gas phase. [13] Oxygen reduction on Pt is regulated by equation (1) [23] and mainly occurs at the catalyst top surface, whereas direct Si etching follows equation (2) and mainly occurs at the catalyst/substrate interface. The balanced equation (3) is given by the combination of equations (1) and (2):



where (s), (l), and (g) indicate the solid, liquid, and gas forms of the molecules, respectively. The process is usually realized at temperatures higher than 45 °C to reduce the condensation of liquid (evaporated HF from the liquid tank or water produced as a by-product) on the surface of etched silicon nanostructures. If the rate of charge carrier injection from the oxidant's reduction exceeds the rate of atom removal by the etchant, the excess holes diffuse away

from the catalyst site, causing undesirable etching at locations that are not in direct contact with the catalyst. For a successful MacEtch process hole injection and mass transfer of the reactants must occur in a uniform manner at every catalyst site and during the full process time. If this is not the case, etch speed differences might cause distortions of the pattern and degrade the pattern transfer fidelity. Because reaction (1) occurs at the catalyst surface and reaction (2) occurs at the interface between silicon and the metal surface, the catalyst surface and interface quality are of crucial importance. [24] Impurities clogging the catalyst surface or the interface between the catalyst and the Si substrate might limit the charge carrier production and injection. Pinning of the catalyst has been reported in MacEtch to induce 3D spiraling movement of the catalyst [15, 25] whereas a cycled variation of oxidant concentration can induce zig-zag structures [26] with a cycled variation of the etching direction. Controlling the etching direction is the key to achieve the highest fidelity of pattern transfer in HAR silicon nanostructures, with the best catalyst path movement being perpendicular to the substrate. Previous work demonstrated that in the gas phase, the reactants can be supplied continuously from an - considering the timescale - infinite reservoir: HF is evaporated from a liquid tank not in direct contact with the catalyst-patterned sample, and  $O_2$  is supplied by air continuously entering the etching chamber. In the gas phase, the oxidant concentration can be much smaller than that of a typical wet MacEtch, so that the porosity of the etched structures, caused by excess holes, can be drastically reduced. [27] A local variation in hole injection can cause a local variation in the etching speed and direction with a consequent distortion in the vertical path of the catalyst movement. Due to the lower concentration of gas reactants [28] in the vapor with respect to the liquid solutions, any local imperfection or the presence of impurities that can alter the MacEtch reaction are more critical in the gas phase than in the liquid phase.

With the progressive moving of the catalyst pattern down into the substrate, the diffusion of reactants through the etched structure becomes the limiting factor to supply a constant and uniform amount of reactant at the catalyst side. We demonstrated that nanowires with aspect ratios of up to 10'000:1 [13] can be realized by self-assembled catalyst patterns, indicating that reactant diffusion is not the limiting factor for this aspect ratio. A much lower aspect ratio has been reported with lithographically patterned nanowires and the same etching method [29] indicating that pattern transfer is critical and is responsible

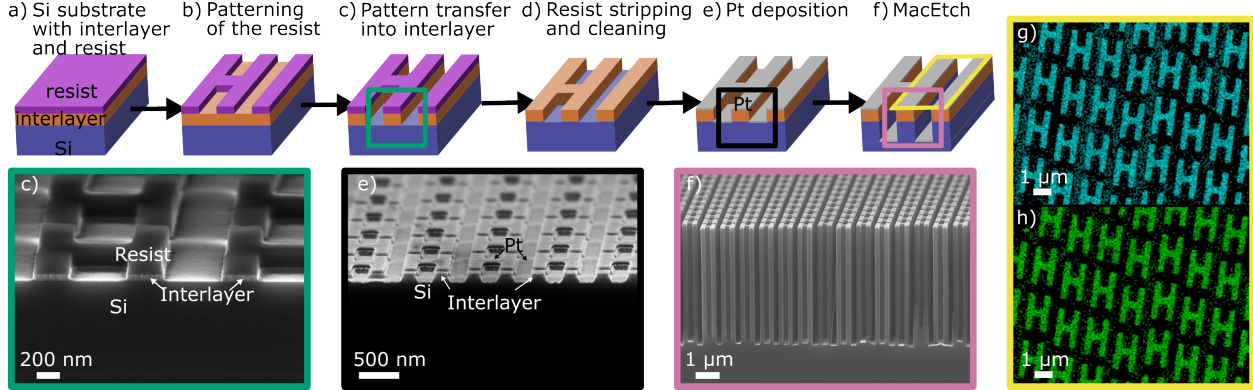


Figure 1: a)-f) show the schematic process flow of the I-Et approach to patterning. The text describes the process flow. SEM images in cross-section (i-k) are given for 3 selected steps. Top-down EDX images are provided for platinum signal (g) and the Cr interlayer signal (h) after MacEtch.

for introducing defects, preventing the realization of HAR nanostructures with a lithographic design. A typical method for lithographically patterning a catalyst is through a lift-off process. In this process, a catalyst is deposited on a developed resist, then the resist is removed by solvents lifting off the catalyst so that only the catalyst deposited on resist free area are left on the silicon substrate. Any residual resist remaining in place and in contact with the catalyst is detrimental to the MacEtch process. [24, 30] Oxygen plasma treatment prior to deposition is required to reduce the amount of residue at the cost of degrading the profile of the patterned resist. [31] Noble metals are usually deposited by physical evaporation, implying a substantial warming of the resist surface during the deposition, which might result in resist reflow or decomposition, leading to a poor yield of the lift-off process (see Supporting Information), [32] especially for feature sizes in the submicron regime. On top of this, Pt also has a very poor adhesion to Si, which often leads to delamination, especially in solvents. [33, 34] The standard way of circumventing this is with adhesion layers. Such layers would block the interface and are therefore not possible in MacEtch. Owing to the prevalence of these issues, many methods have been developed to overcome the yield issue of lift-off, including direct electrochemical nano-imprinting, [24, 35], flow-enabled self assembly of block co-polymers [36], electron beam deposited carbon masking, [37] resist masking, [38] nano-imprint with an undercut layer, [39, 40] patterning of a seed layer and subsequent electroplating of the catalyst [32], shadow masking the deposition of the catalyst [41] and stamping. [42] While these methods manage to circumvent lift-off, they either do not allow for patterning freedom at the nanoscale (elec-

trochemical nano-imprint, flow-enabled self assembly, masking) or fail to effectively separate the resist from the catalyst (carbon and resist masking, nanoimprint, electroplating, stamping).

MacEtch of nanostructures created with a common lift-off approach often leads to inconsistent and random etching, presenting local distortions and tilting of the catalyst pattern at the beginning of the process. In contrast, structures created without the use of a resist do not have these issues, showing very robust patterning integrity even after long etching time with an extremely high reproducibility yield over a very large range of etching conditions. [13] These observations suggest that lithography is the main cause of the poor pattern transfer fidelity in MacEtch. The culprit is hypothesized to be the contamination of the surface that remains after development and before catalyst deposition. [43] Such contamination would affect the MacEtch process. Even electron beam-induced deposition of carbon has been reported as a mask for MacEtch. [37] To prove this hypothesis, we need to separate the resist layer from the catalyst layer by using an alternative to the classical lift-off method to pattern the catalyst. In this study, we introduced an additional layer, that is inert for the MacEtch process, henceforth called "interlayer", between the resist layer and the catalyst layer, eliminating the eventual contamination of the resist residuals by means of a physical separation. The interlayer serves as a medium to pattern the catalyst on clean Si by allowing the substrate cleaning before catalyst deposition. We developed two patterning methods in the presence of chromium (Cr) or aluminum oxide ( $Al_2O_3$ ) acting as physical separator between the Pt catalyst and the Si substrate. Figures 1 and 2 describe the essential workflow of these two approaches.

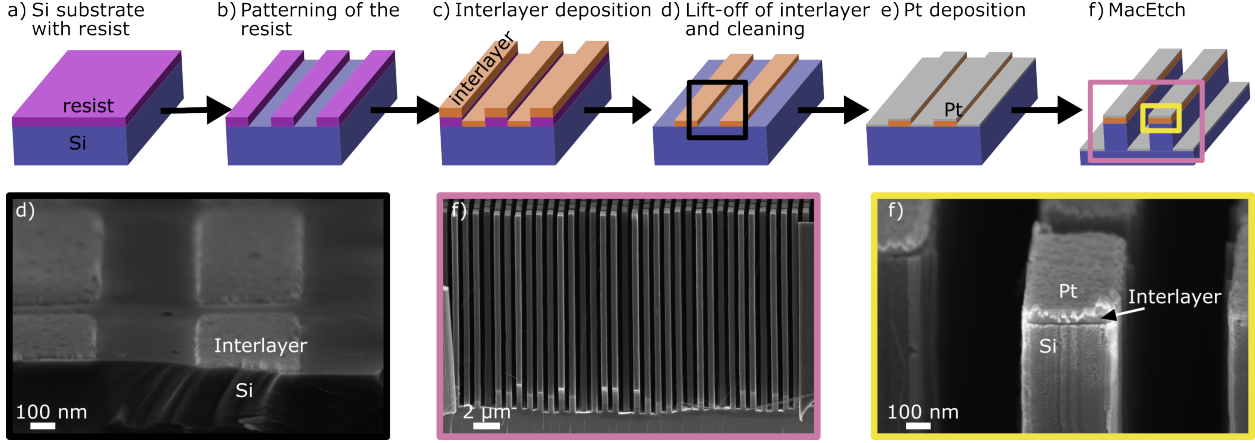


Figure 2: Schematic process flow of the I-Lo approach to patterning. Cross-sectional SEM images of the selected steps with  $\text{Al}_2\text{O}_3$  as the interlayer material.

Examples of dense nanostructures, such as optical elements for X-ray imaging applications [44] with feature sizes in the range of 100-400 nm and aspect ratios higher than 250:1, are realized by MacEtch in the gas phase, demonstrating high levels of uniformity, etching consistency, and pattern integrity.

## Results and discussion

The presence of an interlayer requires an additional step to transfer the pattern from the lithographically shaped resist to the catalyst layer. We present two distinct ways to prepare the pattern by etching (I-Et) or lift-off (I-Lo) of the interlayer material. The later sections cover MacEtch optimization on selected examples. Pattern design and technical details of the processing are described in Materials and Methods. Standard approaches of lift-off and plasma etching to prepare the catalyst pattern are reported for comparison in the Supporting Information.

### Interlayer pattern transfer by etching

Figure 1 illustrates the interlayer etching (I-Et) process flow and its characterization in cross-section scanning electron microscopy (SEM) and Energy Dispersive X-ray analysis (EDX). First, a Si substrate is coated with an interlayer material, here Cr, and a resist. The resist is patterned via electron beam lithography, and the resist pattern is then transferred to the interlayer via plasma etching (Figure 1.c).

This method facilitates the complete removal of the resist layer prior to the deposition of the catalyst. Cleaning can be performed after pattern transfer to the interlayer using oxygen plasma and chem-

ical agents. Cr is an attractive choice for the interlayer because it has been shown to act as a MacEtch block [39, 45-48] and is chemically stable during the process used to develop and strip the resist. This enabled the full removal of the resist without significantly attacking the interlayer. Moreover, Cr has good stability in HF vapor, allowing it to remain during MacEtch. The cleaning process with oxygen plasma before the Pt deposition minimized the catalyst pinning [15] and etch non-uniformities, which could lead to catalyst deformation and uncontrolled etching. A cross-sectional SEM image (Figure 1.f) shows the results of the I-Et method with 50 nm of Cr after 15 min of MacEtch at 55 °C above HF [25%]. The resulting Si structure is an H-bar pillar with a linewidth of 200 nm and a height of 4.8  $\mu\text{m}$ . A clean interface between the catalyst and substrate allows for a consistent and straight etch (Figure 1.f). The EDX images in Figure 1.g-h demonstrate that both the patterned interlayer and the Pt layer atop it remained intact following the etching process. The presented EDX data comes from a 400 nm linewidth structure that was etched with an I-Et method with 50 nm of Cr after 15 min of MacEtch at 50 °C above HF [25%]. The etched depth of the structure was measured by SEM and is approximately 7.6  $\mu\text{m}$ . The observation of Cr and Pt signals on top of the structures substantiates that the employed method results in structures with a tip composed of two layers: the interlayer material (Cr) and the catalyst (Pt). Furthermore, the SEM cross-sectional image (Figure 1.k) shows the efficacy of the Cr layer in obstructing the MacEtch process, as evidenced by the negligible etching observed beneath the Cr interlayer. This finding demonstrates that Cr has MacEtch-blocking capability.

ity not only in wet MacEtch with  $\text{H}_2\text{O}_2$  as the oxidant [45] but also in the gas phase with  $\text{O}_2$ .

## Interlayer pattern transfer by lift-off

The lifting-off of the interlayer provides an alternative for patterning the interlayer. This method avoids the use of plasma processes by employing only liquid chemicals. The corresponding interlayer lift-off (I-Lo) process flow is illustrated in Figure 2. First, the pattern is written on a resist layer coating a Si substrate; the interlayer material is then deposited by physical evaporation methods; the interlayer is subsequently removed by lift-off using a chemical that dissolves the resist layer; after cleaning the patterned interlayer, the catalyst is deposited; and finally, the pattern is transferred into the Si substrate by MacEtch.

Analogous to the I-Et approach, the I-Lo approach facilitates the removal of the resist before catalyst deposition. The process flow allowed for comprehensive cleaning (Figure 2.d) prior to Pt deposition. Using the I-Lo method, materials that are difficult to etch by the plasma process can be used as interlayers, including multilayers. The latter feature enables engineering of the interlayer, by creating a stack comprising one material that acts as a MacEtch blocker and another that imparts functionality to the stack. As an option for an additional interlayer material, we present here  $\text{Al}_2\text{O}_3$  (see SEM in Figure 2). Similar to Cr,  $\text{Al}_2\text{O}_3$  is resistant to oxygen plasma. As an oxide layer, it is compatible with a larger selection of processes and applications, and is CMOS-compatible. Previous studies have used  $\text{Al}_2\text{O}_3$  as a stopping layer for HF vapor etching of  $\text{SiO}_2$ . [49] In our study, we see that it is also able to block MacEtch. In liquid MacEtch, aqueous HF rapidly consumes  $\text{Al}_2\text{O}_3$ . [50, 51] In contrast, in gas MacEtch,  $\text{Al}_2\text{O}_3$  will survive as HF vapor does not attack  $\text{Al}_2\text{O}_3$  in a significant manner. [50, 52] This enables the use of  $\text{Al}_2\text{O}_3$  as an attractive blocking layer for gas-phase MacEtch. We demonstrate here the  $\text{Al}_2\text{O}_3$  interlayer properties by etching nanostructures for 30 min at 60 °C above HF [50%] with a linewidth of 400 nm and an etching depth of 15  $\mu\text{m}$  (Figure 2.f). The metal oxide tip ( $\text{Pt-Al}_2\text{O}_3\text{-Si}$ ) is clearly visible in the high-magnification SEM image of the top part of the etched grating (Figure 2.f). Compared to the I-Et method, I-Lo provides a universal solution that does not require selective etching of multiple layers. This enables the use of any stack of materials that survive the exposure to HF vapor and has one layer of blocking MacEtch. In correspondence to the I-Et approach, no significant undercut or erosion is observed on the top surface (Figure 2.i), as expected for anisotropic etching by MacEtch

in gas phase, where the injection of charge carriers by the oxidant reduction can be tuned much better than in liquid reaction. With respect to Cr,  $\text{Al}_2\text{O}_3$  is more compatible to thermal treatments, such as the one needed for Pt-dewetting to create a porous catalyst layer. [13] In contrast to the I-Et approach, in which the lithographically exposed areas undergo etching, in the I-Lo approach, the exposed areas are blocked by the interlayer. Thus, the I-Lo approach represents a quasi-inverse lithographic process compared to the I-Et approach. I-Lo and I-Et can be combined as a function of the required pattern, providing complementary designs for a more efficient lithography process. In direct-writing lithography, the proper choice of patterning can be relevant to reduce the processing time, in particular for large area patterns. The same resist can be used for both methods, which simplifies the writing and enables the use of the preferred resist for both approaches, irrespective of positive/negative tone of the resist.

## Enhanced interlayer profile

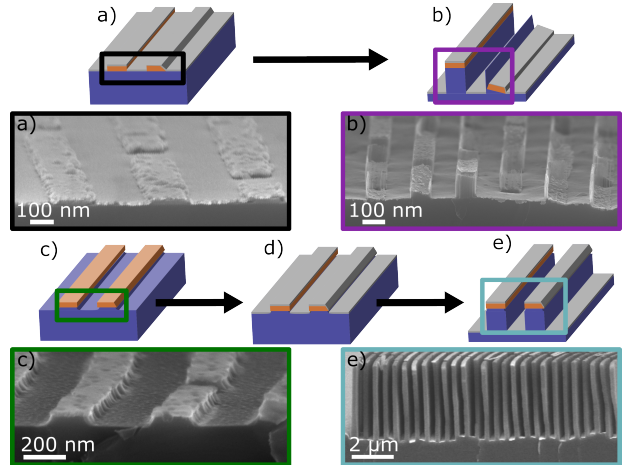


Figure 3: A schematic showing the issue in pattern transfer arising from a poor interlayer profile (a-b), solved by 20 nm plasma etching of Si using the interlayer as hard mask (c-e). The supporting cross-sectional SEM images show select steps in the process.

The success of the interlayer method relies on successful catalyst separation during deposition. If the catalyst on the interlayer is connected to the one on the Si, it impedes sinking during MacEtch. The result of such a situation is a poor pattern transfer with defects, high porosity, and/or destroyed tops, as seen in Figure 3 b. During MacEtch, the catalyst will either be blocked or sink and drag the top with it.

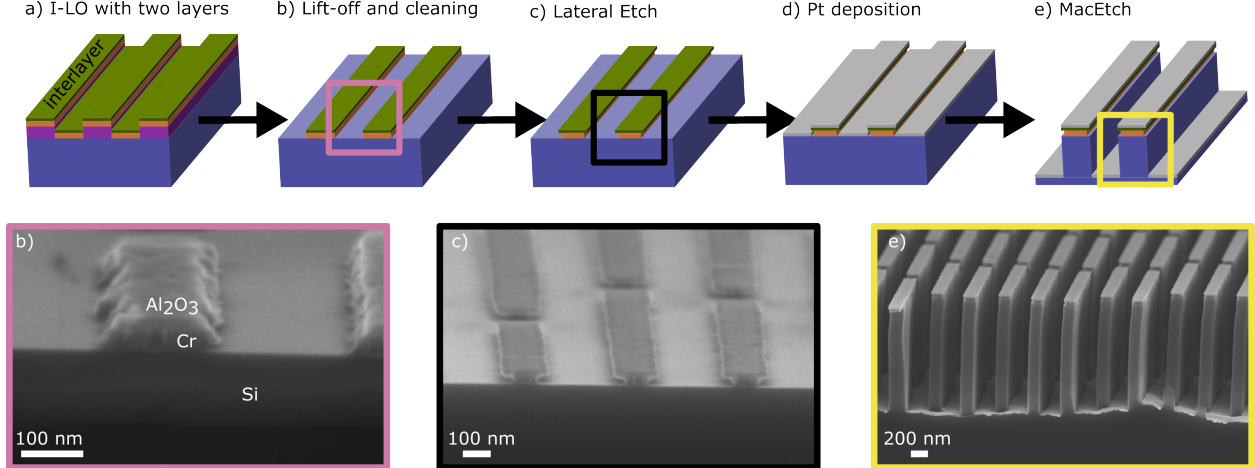


Figure 4: A schematic showing an advanced process using a bilayer as the interlayer to create an undercut. The scheme proceeds as I-Lo, followed by a selective lateral etch of the lower layer before the deposition of Pt. h)-j) show cross-sectional SEM images of the selected steps of the process with Cr/Al<sub>2</sub>O<sub>3</sub> as the interlayers.

In both cases it will inject charge carriers from the side to etch the structure laterally. If the catalyst sinks with the top, one side of the structure remains, leaving behind characteristic fences and a sunk top (Figure 3.b). To avoid this, the interlayer should have straight sidewalls or even an undercut before catalyst deposition. [39] This can be achieved with both the presented interlayer methods by optimizing the process for the interlayer profile. If this is not possible or only with a low yield, enhancements of the interlayer can be performed to ensure such an undercut with the help of a second layer. A solution is shown in Figure 3 c. Isotropic etching of Si creates an undercut in the Si layer (Figure 3.c). Using a SF<sub>6</sub>/O<sub>2</sub> plasma treatment, we etched 20 nm of Si using the interlayer as a hard mask. Such a small artificial undercut leaves the top of the structure with minimal damage. This undercut disconnects the catalyst after deposition (Figure 3.d), removing the defects of poor pattern transfer (Figure 3.e). The example structure was etched for 10 min at 55 °C above HF [50%] (Figure 3.c).

Alternative to silicon etching, one can use a multilayer consisting of two materials with the ability to etch one selectively over the other to create an undercut layer. We report here an example with a double layer of Cr and Al<sub>2</sub>O<sub>3</sub>. The process is outlined in Figure 4 for the I-Lo approach, with supporting cross-sectional SEM images. It starts with the exposure of the resist followed by the deposition of a bilayer of Cr/Al<sub>2</sub>O<sub>3</sub> as the interlayer (Figure 4.a) and subsequent lift-off (Figure 4.b). In this step, the sample is cleaned from resist residuals. The undercut is then

created by immersing the sample in a diluted solution of Cr etchant to achieve lateral etch rates in the nm/s regime. The result is a clearly defined undercut in the Cr (Figure 4.c). A plasma process to undercut Cr is also available (See Supporting Information). The catalyst is then deposited (Figure 4.d), and MacEtch performed with this structure (Figure 4.e). The presented cross-sectional SEM image shows the result of a grating etched at 50°C for 15 min above HF[37.5%]. Using a liquid etchant, this method also remains an option for creating MacEtch structures without the use of a plasma, even if an enhanced undercut is required.

The optimization of the etching conditions for the different structures has been determined in a systematic study. We observed the etch rate as a function of different parameters and - more importantly - the etch quality. Figure 5 shows the corresponding results for the I-Et method. For the etch quality, we investigated the catalyst profile at the bottom of the etched trenches and we separated the results into three different categories based on the catalyst quality and structural cohesion. In Figure 5.d-f three examples of different catalyst qualities are presented. The requirement for successful pattern transfer is a straight sinking of the catalyst without isolated deflection from the vertical direction into the substrate. This translates into a catalyst layer that remains intact at the end of the process. Therefore, we accept catalysts that are wavy (Figure 5.e) but not those that are disconnected (Figure 5.f). These criteria were used to determine the best etching results for different concentrations and shapes. For comparison,

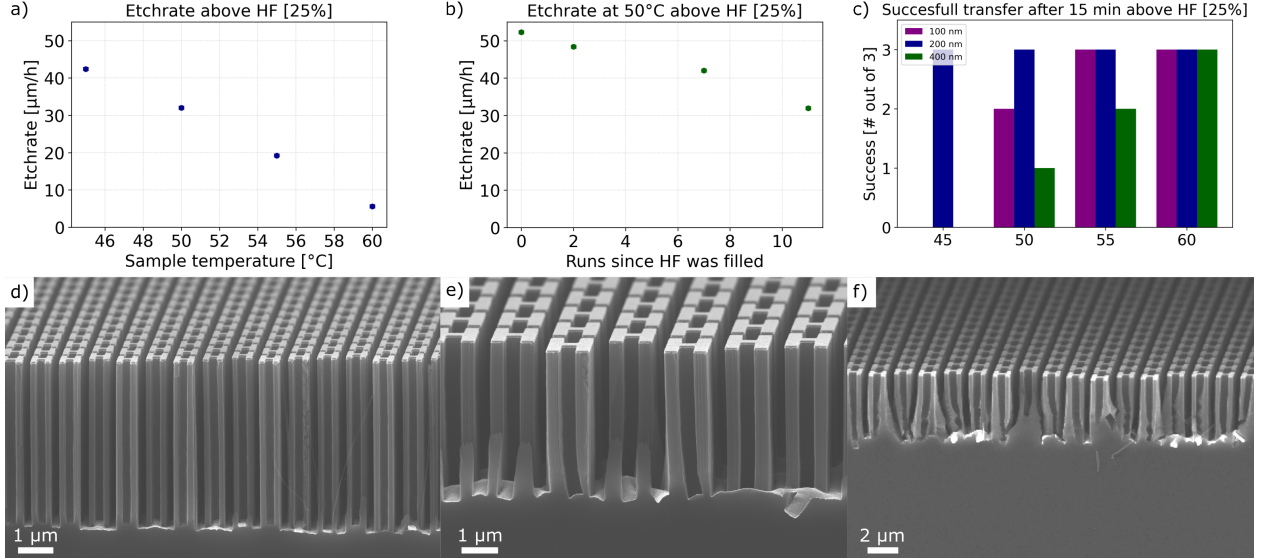


Figure 5: Etch rate of H-bar structures with 200 nm linewidth as a function of a) number of runs (opening the pot and letting the vapor out-diffuse) and b) sample temperature. c) sweep of four sets of consecutively etched samples using the I-Et method (H-bar structures with different linewidth asa indicated). The structures were sorted according to the catalyst quality. SEM in cross-section of three examples with different qualities of the catalyst at the bottom of the etched trenches: d) a catalyst layer with good quality, e) a wavy catalyst without tears, and f) catalyst with isolated motions and breaks.

we took all identical samples treated on the same Si wafer and cleaved them in chips before MacEtch. The chips were etched sequentially with a short break between them. The difference between the samples was the temperature at which they were held during etching, which was performed in a randomly chosen order of 45, 55, 60, and 50 °C. The etching rate decreases as a function of the etching temperature (Figure 5.a) and a quality trend emerged, showing better transfer with increasing temperature (Figure 5.c). The reduction in etch speed with increasing temperature can be attributed to the lowered adsorption of water on the surface. Water adsorption has been reported to catalytically support the HF removal of  $\text{SiO}_2$  in the vapor-HF process. [53] We can then assume that water reduction can also slow down the MacEtch process, despite MacEtch being thermally activated. [54] This behavior was also observed in the shape of a volcano plot in a previous work. [13] Furthermore, the comparison of etch rates for MacEtch in the gas phase is a very challenging task due to the difficult control of the reactant concentration. For small areas and short etches, we can neglect the etchant consumption during the etching itself. Instead, the main loss occurs when the system is opened, and the formed HF vapor can escape the chamber. This was investigated by plotting the etching rate measured for identical samples under the same etching conditions at a tem-

perature of 50 °C for 15 min above the HF [25%] as a function of how often the system was opened after at least 15 min of evaporation (Figure 5.b). This high sensitivity of the etch rates to the HF concentration shows that control of the etching conditions is crucial for reproducible results. This indicates the requirement to replace HF frequently to obtain comparable data from this setup. Therefore, we refrain from providing comparative data with samples that did not have controlled concentrations.

Interlayer patterning can solve the challenge of etching large area dense patterns (grating with duty cycle of 0.5), which have so far proven challenging with MacEtch. Good ultra-high aspect ratio pattern transfer in silicon using MacEtch with vapor HF have only been reported for small areas and nanowire patterns. The interlayer method achieved consistent etching over an area of 1 cm<sup>2</sup>. Figure 6 shows the depth profile of a 200 nm line grating created with I-Et and SEM images in cross-section of selected positions. The depth profile was obtained by carefully measuring the SEM images in the cross-section at a defined distance from the edge of the sample. The etched samples were patterned together using the I-Et method on the same wafer. All samples had the Cr interlayer removed in a liquid etchant to enable dewetting, a process that improves the mass flow through the catalyst. [13] In the first run, the 0.4 cm

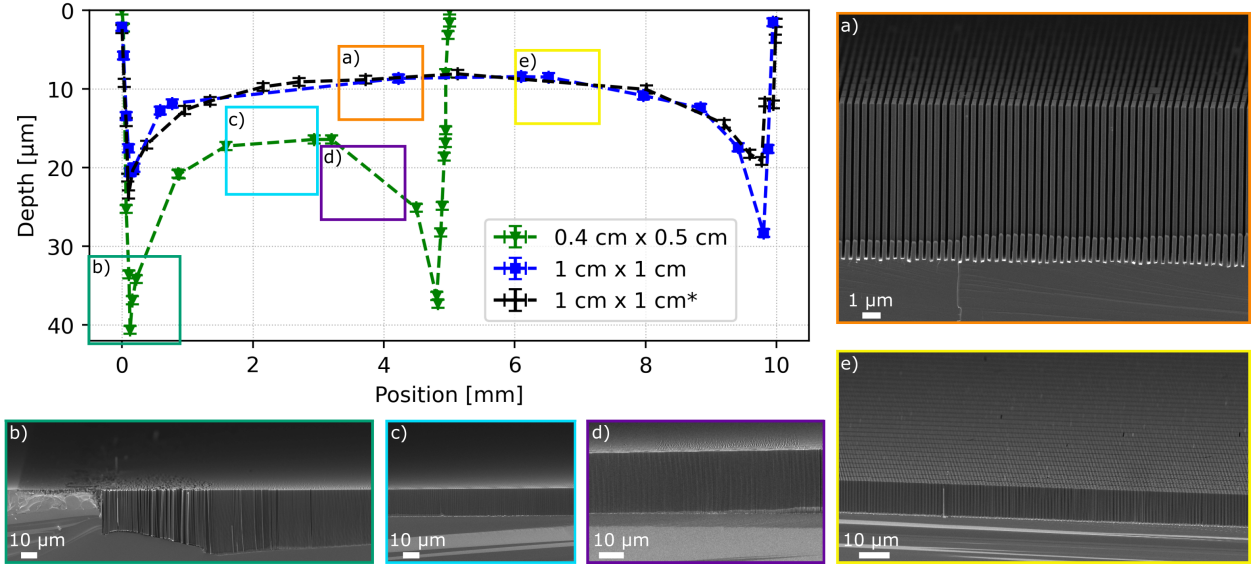


Figure 6: Etching depth of three samples of 200 nm line grating created with I-Et method and subsequent MacEtch as a function of the position in the pattern. The dashed lines serve as a guide for the eye. The legend denotes the dimensions of the patterned area. All the samples were etched under the same conditions: etching for 1 h at 50 °C over HF [25%]. The sample marked with \* was etched 2 months later. The depth profile was reconstructed with the help of SEM images. The squares show selected SEM images in the cross section at different locations of the dewetted gratings.

$\times 0.5$  cm area sample was etched together with a  $1\text{ cm} \times 1\text{ cm}$  area sample, which were both dewetted at 350 °C for 1h. The second sample with  $1\text{ cm} \times 1\text{ cm}$  area was etched two months later without prior dewetting (see Supporting Information). All the samples were etched for one hour at 50 °C over HF [25%]. To make the results comparable, we used a freshly mixed solution for both samples.

The etching is faster at the edges of the patterned areas, a sort of microloading effect due to a local depletion of the reactants in the region with high pattern density, occurring also in plasma etching. [55] The depth of the structures changed continuously throughout, with no relevant breaks in the catalyst apart from the edge. As the utilized method is I-Et, the outsides of the patterned area do not contain an active catalyst site. Hence, the unpatterned area do not consume reactants during MacEtch, resulting in a gradient of reactant concentration decreasing from the edges towards the center of the pattern. Being an edge effect, it is sensitive to the sample area; in fact, the  $1\text{ cm} \times 1\text{ cm}$  sample (Figure 6) has a more uniform etching in the center as the distance from the edge is larger. The larger the pattern area the larger the consumption of reactants, leading to an overall slower etch rate (loading effect), such that the larger sample reaches a 20–30  $\mu\text{m}$  etching depth at

the edges with respect to the 40  $\mu\text{m}$  of the small sample. Similar edge effects have been reported for MacEtch in liquids [56] and gases. [13, 26] However, in L.L. Janavicius et al. [26] both etchant and oxidant gases flow across the sample, with one side of the sample facing the flow (leading side). In our system the HF is evaporated perpendicular to the sample, while the O<sub>2</sub> flows into the chamber from all the lateral sides of the sample. The etching profile appears symmetric, some minor difference at the edges can be related to the omission of the proximity effect correction in the lithographic step, which affects the first tens of  $\mu\text{m}$ . [57]. The decrease of the etch rate with the sample area could be counterbalanced with an increase in reactant flow. Due to the tool limitations, this is not further investigated here. The etch depth was successfully replicated in a second experiment two months later. Reports about consistency in the previous literature regarding samples prepared by MacEtch are quite limited. Therefore, a comparison with other studies is difficult. Figure 6 shows that we can reproduce the same etching profile with high accuracy of etch depth by processing two samples, even two months apart. The key reason is the consistency of the experimental parameters, such as the replacement of the HF solution prior to each experiment and a clean pattern transfer. The dewetting

step seems to be irrelevant, indicating that for these feature size, the HF can reach the Si underneath the catalyst by diffusing from the catalyst borders.

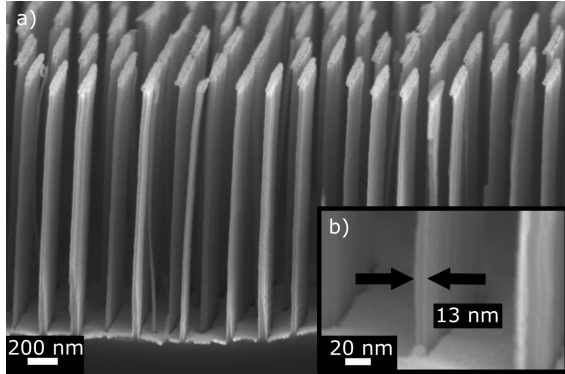


Figure 7: Cross-sectional images of MacEtch samples, showing thin Si lamellas. a) wider view of the fin structure fabricated with I-Lo using Cr/Al<sub>2</sub>O<sub>3</sub> and etched 15 min at 50°C above HF [37.5%]. b) Zoomed image of the structures, demonstrating fin width of 13 nm width and very little lateral etching.

With an unpatterned mesoporous catalyst we estimated a feature size limit for gas-MacEtch around 10 nm. In our previous work [32], we observed very thin lamellas but the lateral etching was predominant, compromising the structural stability of the Fins. Here, we report patterned structures with linewidth in the range of 10 nm realized by I-Lo and advanced undercut of Cr/Al<sub>2</sub>O<sub>3</sub> interlayer. The structure is very sensitive to the etching conditions (see Figure 7.a) because even slight sideways etching is sufficient to release the structure. The lamellas are as thin as 13 nm (see Figure 7.b) with a very smooth sidewall. The Pt catalyst at the bottom of the Fins shows a minimal gap in the nanometer regime to the sidewall, demonstrating the almost negligible lateral etching of MacEtch in gas phase in the single-digit nanometer range, which could potentially lead to etching conditions with zero-roughness - a very attractive feature for photonic devices in quantum technologies [58]. With this, the final limit of resolution achievable in the etching is even below 10 nm, in line with previous observations in wet-MacEtch. [59]

## High aspect ratio structures

Metal assisted chemical etching has shown the ability to etch samples to considerable depth regardless of feature size. The improved patterning process with more consistent etching allows achieving a large etching depth in high aspect ratio structures with a high level of control. Both the I-Et and I-Lo methods can

be used to create high aspect ratio structures. In Figure 8 we present a selection of optical elements that highlight the capability and flexibility of MacEtch. Conventional fabrication of these structures at this aspect ratio is challenging or impossible with more established etching methods, highlighting the advantages that MacEtch can offer. These structures could all be etched with a higher aspect ratio and functional tops, given sufficient optimization (see Figure 9). Diffractive Optics in the X-ray regime usually require high precision ordered vertical structures with submicron feature size and high aspect ratio, [60, 61] due to the high transparency of materials to X-rays. Circular gratings are regularly used in X-ray Optics in the form of Fresnel zone plates [62] with varying zone widths or in arrays, as here, to impress a phase variation in the wavefront, useful to detect directional features such as in X-ray tensor tomography [63]. Checkerboard patterns with single [64] (Figure 8.b) or multiple pitch [65] (Figure 8.d) are used as optical elements in grating interferometry. Figure 8 a) shows an array of circular gratings etched to a depth of 3.5  $\mu$ m. The grating was etched for 30 min at 50°C above HF [37.5%] and has a small pitch of 460 nm and a large pitch of 50.6  $\mu$ m. Figure 8 b) shows a checkerboard grating etched for 30 min at 50°C above HF [37.5%] with a pitch of 400 nm. Figure 8 c) shows a ring resonator etched for 30 min at 45°C above HF [37.5%] with a pitch of 600 nm and an opening of 85 nm, demonstrating a structure with a hollow center. This is the closest to a via that is possible while keeping the catalyst connected, which is a requirement. [59]

Figure 9 shows cross-sectional SEM images of various structures with a feature size of approximately 200 nm and depth of approximately 50  $\mu$ m created with I-Et and I-Lo.

Shown are a h-bar structure (linewidth 200 nm) created by I-Et that was etched for 3h at 55 °C above HF [12.5%] (Figure 9.a); an h-bar structure (linewidth 200 nm), created by I-Lo, etched for 30 min at 50 °C above HF [50%] (Figure 9.b); a checkerboard pattern (linewidth 200 nm), created by I-Lo, etched for 60 min at 50°C above HF [50%] (Figure 9.c); an I-Lo double checkerboard grating (P1: 3.6  $\mu$ m; P2: 400 nm) etched for 60 min at 50°C above HF [50%]. Both I-Et and I-Lo patterning methods can etch 200 nm linewidth h-bar structures to a depth of 50  $\mu$ m. The checkerboard pattern shows the possibility of very deep etching (53  $\mu$ m) with a 50% dense structure. The double checkerboard shows the ability to etch deep structures (40  $\mu$ m) with masks of the two different sizes in the same pattern, the wavy catalyst pattern at the bottom of the trenches

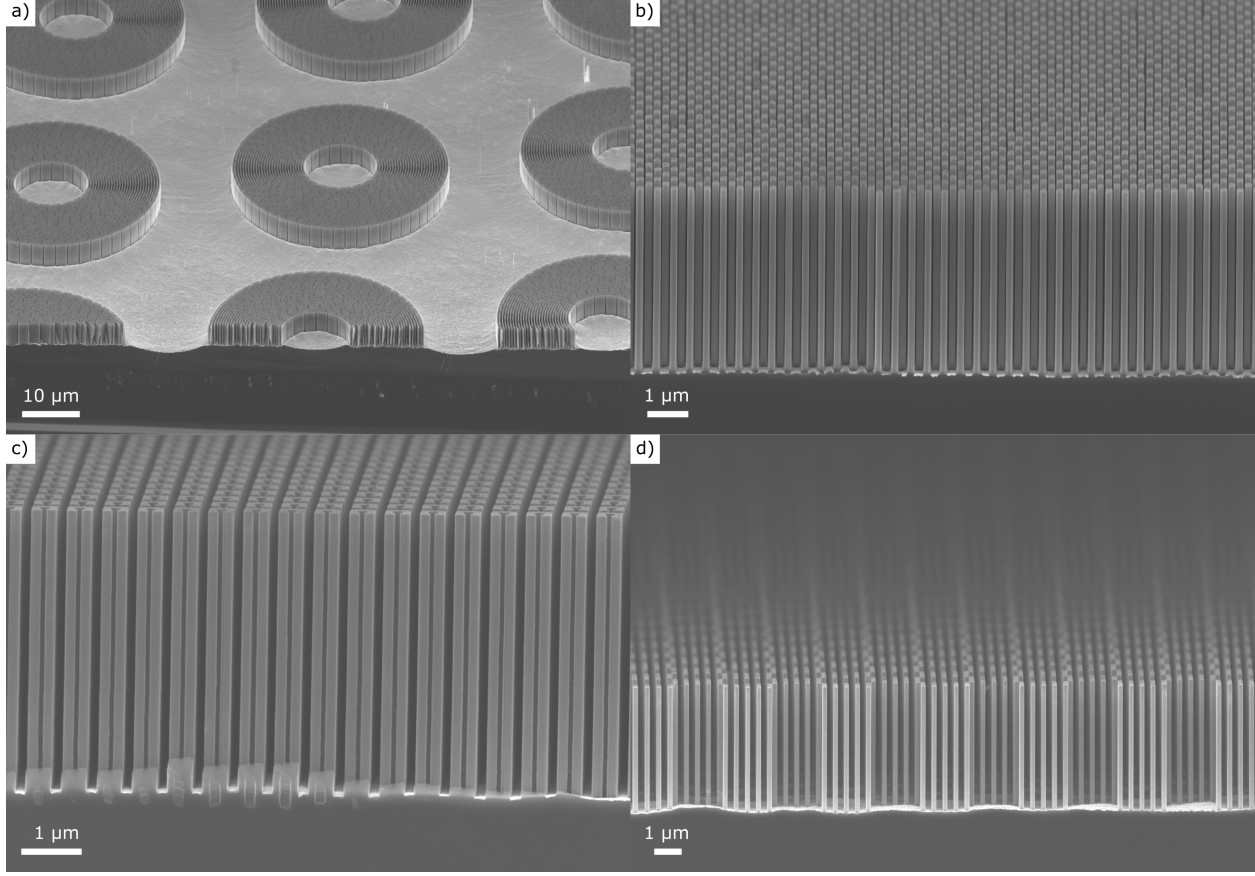


Figure 8: Cross-sectional SEM of various structures created with the I-Lo method etched for 30 min above HF [37.5%]. a) ring grating etched at 50°C with a small pitch of 460 nm and large pitch of 50.6  $\mu\text{m}$  (SEM tilt of 30°); b) checkerboard grating etched at 50°C at 30° stage tilt; c) ring-oscillator structures etched at 45°C with an opening of 85 nm and pitch of 300 nm (SEM tilt of 10°); d) double checkerboard etched at 50°C with a small pitch P1 of 400 nm and a large pitch P2 of 3.6  $\mu\text{m}$  (SEM tilt of 10°).

indicates a very minor dependence of etch rate on the pitch size (Figure 9.d). The achieved etching depth and the resulting aspect ratio of over 250:1 are in the same regime of the self-assembled pattern from dewetting. [13] The structure all etch predominantly straight with smooth sidewalls. This shows a clear advantage compared to the etching in plasma, in which sidewall roughness, tapering, aspect ratio dependent etching rate such as ARDE and RIE-lag are well-known drawbacks [66]. In particular, for applications such as meta-lenses [37, 67] and photonic nanocavity [58], where a uniform structure height and sidewall smoothness are needed for a variety of different feature size, MacEtch in gas phase can be an attractive alternative.

Some of the h-bar structures in the sample processed using the I-Et method look extruded (Figure 9.a). In this example, the catalyst exhibited uneven and uncontrolled etching at the bottom of the

grating trench. The etching conditions of this sample were set in a low HF concentration (HF [12.5%]) to reduce the etching rate, as faster etching is not sustainable for this I-Et pattern. MacEtch has been reported to etch different crystallographic directions and the switching from the main etching direction of  $<100>$ , which is the wafer surface, is mainly dictated by the etching rate [54]. If the etch front reaches this regime, for example by locally unbalancing the HF/O<sub>2</sub> ratio, the etching proceeds in a different direction and chaotic etching occurs, which breaks the catalyst. This happened at the bottom of the structure after a straight etching of about 50  $\mu\text{m}$ , and the structure is subsequently extruded. Assuming to be in conditions of high HF concentration, the catalytic decomposition of the oxidant becomes the rate determining process. In the I-Et (Figure 9.a) sample, the area external to the pattern has blocked catalyst and the active catalyst area is 50 times smaller with

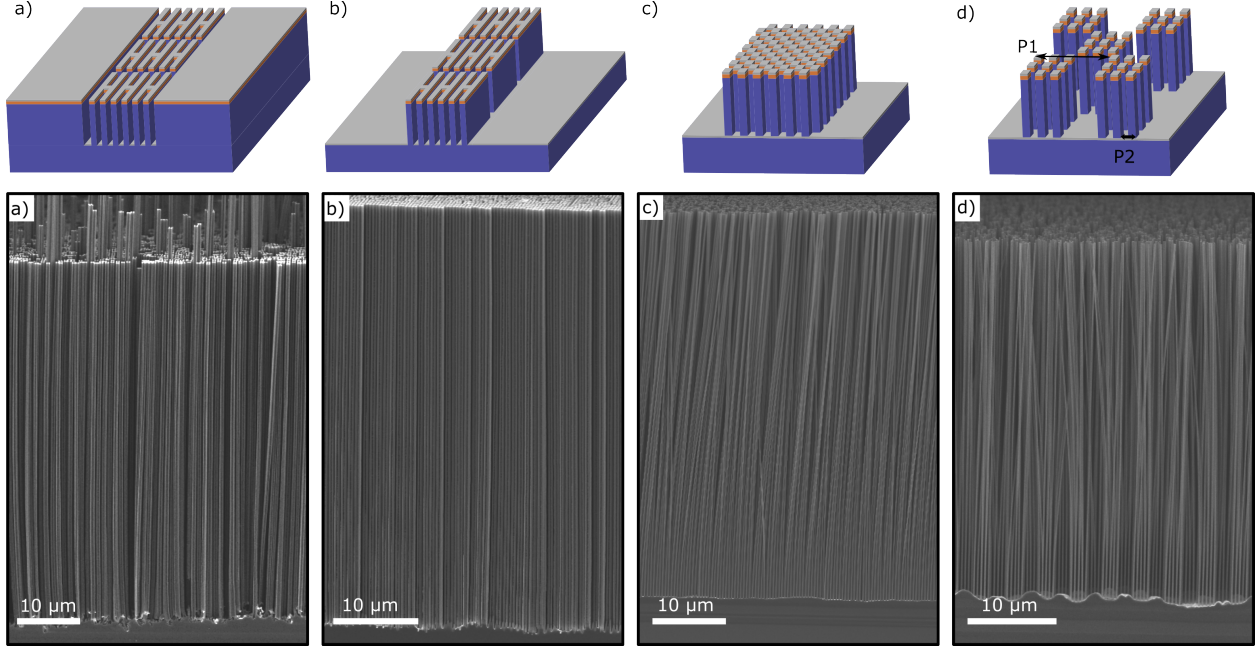


Figure 9: Different schematics and cross-sectional SEM images of high aspect ratio structures. a) h-bar grating created with I-Et, the sample was etched 3h at 55 °C above HF [12.5%]; b) h-bar grating created with I-Lo, the sample was etched 30 min at 50°C above HF [50%]; c) checkerboard grating created with I-Lo, the sample was etched 60 min at 50°C above HF [50%]; d) double checkerboard grating created with I-Lo, the sample was etched 60 min at 50°C above HF [50%]

respect to the I-Lo sample. Similarly to the observations regarding the loading effect (see Figure 6), the difference in the active area of the catalyst causes a relevant difference in the consumption of the reactants and hence a different etch speed. Despite us lowering the HF concentration in the I-Et sample and the etching rate being 3 times slower with respect to the I-Lo one, the diffusion trough 50  $\mu\text{m}$  tall structures altered the HF/O<sub>2</sub> balance at the bottom causing an excess of Oxygen, that triggered the onset of etching events in different directions. In comparison, the samples processed by I-Lo were etched with a much higher nominal HF concentration and exhibited an intact catalyst with no structural damage indicating that the dynamic consumption of reactants operated by the larger area of exposed catalyst is more efficient in optimizing the etchant concentration. These examples show the need to adjust the etching concentration for the successful etching of each specific pattern and catalyst active area.

## Conclusion

In this paper, we present novel patterning methods to improve catalyst preparation for MacEtch. A crucial innovation is the introduction of an interlayer material that physically separates the catalyst from the lithographically processed resist. Thereby, reducing the contamination of the catalyst and allowing a more thorough cleaning before Pt deposition lead to a more controlled pattern transfer. We demonstrated two different approaches of pattern transfer in the catalyst layer in the presence of an interlayer material, using the assistance of plasma-based pattern transfer (I-Et) or lift-off (I-Lo). This was supported by two different materials acting as interlayers (Cr and Al<sub>2</sub>O<sub>3</sub>). It has been reported that Cr is a blocking material for MacEtch in HF-H<sub>2</sub>O<sub>2</sub> liquid systems, and we observed the same capability of blocking MacEtch in HF-O<sub>2</sub> gas phase. We also demonstrated that Al<sub>2</sub>O<sub>3</sub> is a good blocking layer for MacEtch in HF-O<sub>2</sub> gas phase. In principle, any material with a different MacEtch behavior than that of the material used as main catalyst is a possible candidate for the interlayer, including those that catalyze the MacEtch process, if the interlayer material has a different etching rate with respect to the main

catalyst. The presence of an interlayer yields an improved catalyst that enables the etching of nanostructures in a controlled manner with smooth and straight sidewalls. We focus on providing a multitude of fabrication options that do not require state-of-the-art tools and can even create nanostructures using only a lithographic tool, a metal evaporator, and liquid chemicals. This also makes Si etching accessible to small laboratories. Additionally, the presented method opens the way for the creation of elongated Si nanostructures with high aspect ratio and retaining a multilayer top coating via MacEtch. The top coating materials can be deposited prior to etching as part of the lithographic process, facilitating the streamline of the process because no second patterning step before etching or deposition after etching are required. The enhanced stability of the catalyst obtained with the novel method was demonstrated by consistently etching gratings of various areas. The improved catalyst was employed to etch 200 nm linewidth gratings of various areas up to 1 cm × 1 cm. The depth profile was carefully measured by sampling the etched depth at different positions, revealing a microloading effect with edges etching faster, as well as a loading effect with sample size dependence of the etching rate. We demonstrated the reproducibility of the same profile even after a few months with the same set of conditions. The high aspect ratio and large-area etching speak for the relevance of the clean catalyst towards a consistent MacEtch process. The criteria for etching optimization were focused on structural quality. A non trivial optimization is needed to achieve high aspect ratio structures of good quality with different pattern feature size and catalyst density, being the reactants depletion the main factor affecting the process stability. In this respect, the HF evaporation tool at atmospheric pressure is limited. A real time detection of the actual reactants consumption and the possibility to regulate the gas flow in a more sophisticated tool could open new possibilities and new optimization strategies. Nanofabrication with extreme resolution (below 10 nm) in silicon pattern transfer and aspect ratios of over 250:1 have been demonstrated in a variety of optical elements useful for applications in the X-ray regime, using both the I-Lo and I-Et approaches. Extreme sidewall smoothness and verticality of the etched features are relevant to control optical manipulation in nanophotonics. Our findings help to understand the relevance of interface chemistry and the fundamental role of catalyst preparation for MacEtch of silicon, contributing to develop the necessary building blocks in upcoming photonic applications, where MacEtch can open new possibilities of nanostructuring in plasma-free processing.

## Materials and Methods

Since the goal is to demonstrate the fidelity of pattern transfer during MacEtch, especially in the direction perpendicular to the substrate, we designed the patterning unit with a functional shape: a large mesh of an interconnected catalyst [13] with a periodic array [68] of units so that the eventual deflection due to the catalyst motion can be easily visualized at low magnification as a defect in the periodicity; a pattern unit that produces silicon pillars with a cross-section of an H bar or rectangles, so that the corners can be easily detectable in cross-section scanning electron microscopy (SEM) with minimal deviation in footprint with respect to circular pillars, which are the most used MacEtch structures. H bars are also more stable in terms of stiction with respect to rectangles in the case of liquid condensation during long etching processes or humidity before the SEM inspection, so this kind of functional pattern is more suitable for investigating very high aspect ratio features.

All samples were prepared on fresh N-type phosphor-doped 4-inch silicon wafers with a  $<100>$  orientation, resistivity of 1-30 M $\Omega$  cm, and wafer thickness of 250  $\mu$ m. Prior to patterning, the wafers were cleaned in oxygen plasma. Cr, Al<sub>2</sub>O<sub>3</sub>, and Pt were deposited using electron beam evaporation with a BakUni system from Evatec. The lithography was performed by electron beam lithography using a Raith EBPG 5000Plus and the positive-tone resist CSAR-62 from Allresist GmbH. The dimensions of the patterned area are 100  $\mu$ m × 2 mm unless mentioned otherwise. This small size reduces the writing time while still allowing for a consistent dicing of the structure along the long side of the structure. Larger patterns were produced to test uniformity (Figure 4). For the resist, the developer AR 600-546 and the remover AR 600-71 from allresist were used, owing to the great resolution and fast removal. For the I-Lo process, we used a process adapted from Ohlin et al. [31] The process consists of an initial soak followed by sonication. The substrates were cleaned using coupled plasma reactive ion etching with O<sub>2</sub>. This removes the remaining resist and etches Si, which further aids in the separation of the layers. In I-Et approach, Cr was etched with Cl<sub>2</sub>/O<sub>2</sub> plasma (1).

The gas-phase MacEtch process consists of exposing the Pt-patterned Si samples to HF vapor and O<sub>2</sub> gas as described in a previous work. [13] During etching, the sample is held in place and in contact with a heated holder at a fixed temperature by physical clamping. For etching, the basin gets filled with aqueous HF. This creates an etching chamber filled

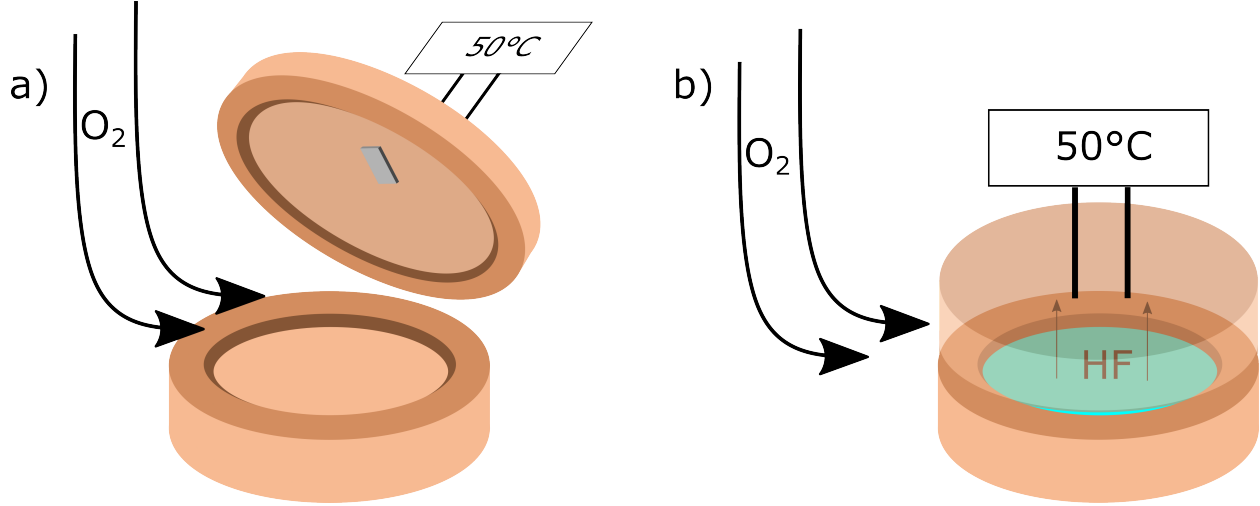


Figure 10: A sketch of the used vapor HF tool from IDONUS. The sample is placed on the top part of the tool a), which can be heated. The tool was then closed, and HF was flown in (b). The sample is held at a distance of 1.3 cm from the liquid allowing HF to evaporate in the chamber and oxygen to flow into from the side.

with air and HF vapor at ambient pressure. MacEtch was performed using the vapor HF tool developed by Idonus (Figure 10), the liquid solution had a fixed total volume of 200 ml and the composition was varied by mixing different volumes of DI water (18 MΩ) and aqueous HF from Technic at 50% volume concentration. The main parameters for this experiment consist of: the holder temperature, giving the sample temperature; the HF concentration in the liquid, giving the HF concentration in the gas; the distance between the sample and the liquid, affecting the vapor concentration at the sample surface; and the etching time. The first three parameters affect the chemistry of the process, and hence the reaction rate, as shown in previous studies. [29] The etch rate increases as a function of HF concentration, presenting a volcano plot as a function of temperature, with a maximum at approximately 45 °C, and decreases as a function of the distance of the sample from the liquid level. In this study, the etching conditions were optimized by varying the temperature in the range of 45-60 °C and the amount of HF 50% in the liquid solution. The total amount of liquid was fixed at 200 ml and made up of a mixture of HF and DI. We use a compact notation for the HF concentration, for example: HF [50%] corresponds to 200 ml HF 50%, HF [25%] corresponds to 100 ml HF 50% and 100 ml DI, and so on. The criteria for etching optimization are focused on structural quality.

The samples were mechanically clamped on the heating holder and held at 1.3 cm from the liquid to be exposed to the HF vapor. The etching time

was determined as soon as the liquid was allowed to flow. One minute before stopping the timer, the liquid flowed out of the chamber, and the process was stopped by removing the top with the sample. The sample was then kept at temperature to eventually allow the HF to evaporate from the sample for safety. The inspection of SEM in cross section was performed by the cleaving the silicon samples. SEM imaging was performed using a Zeiss Supra VP55 under a 10° tilt, if not mentioned otherwise, with an active tilt correction. Any sample accounted for the etch rate plots and profiles had an intact catalyst and at least a locally successful pattern transfer. (See condition in Figure 5)

To remove the tops before MacEtch, the liquid etchant Technietch Cr 01 from Microchemicals GmbH was used. The samples were immersed in the solution and agitated in an ultrasonic bath. Thermal dewetting was performed on a metal-covered hotplate in air for 1h.

The used MacEtch conditions presented in this work are listed in Table 1. We remind the reader that this data is only suited for broad comparison, as the concentration of the liquid and the overall patterned area is varied between the samples.

Table 1: The MacEtch conditions and etching depths of the samples presented in this work and the relative Figures.

Figure	method	HF 50% [ml]	DI [ml]	T [°C]	time [min]	linewidth [nm]	max depth [μm]
1.f	I-Et	100	100	55	15	200	4.8
1.g,h	I-Et	100	100	50	15	400	7.6
2.f	I-Lo	200	0	60	30	400	15
3.b	I-Lo	100	100	45	30	400	0.4
3.e	I-Lo	200	0	55	10	230	3.8
4.e	I-Lo	150	50	55	15	200	1.3
5.d	I-Et	100	100	55	15	200	4.8
5.e	I-Et	100	100	55	15	400	4.3
5.f	I-Et	100	100	50	15	400	4
6.a,e	I-Et	100	100	50	60	200	28
6.b,c,d	I-Et	100	100	50	60	200	40.5
7	I-Lo	150	50	50	15	15	1.6
8.a	I-Lo	150	50	50	15	230	3.3
8.b	I-Lo	150	50	50	15	200	4.5
8.c	I-Lo	150	50	45	15	150	4.8
8.d	I-Lo	150	50	50	15	200	4.6
9.a	I-Et	50	150	55	180	200	53.5
9.b	I-Lo	200	0	50	30	200	50
9.c	I-Lo	200	0	50	60	200	53
9.d	I-Lo	200	0	50	60	200	40

## Acknowledgements

The authors thank the funding agencies: Swiss Nanoscience Institute; the SNI PhD grant MAGNET; PHRT-TT Project Nr. 2022-572 INTIMACY; SNSF grant Nr. 200021-232339 ABSOLUTE; PROMED-ICA Stiftung Chur, Grant Nr. 1788/M. We thank: the PSI cleanroom facilities PICO; K. Jefimovs, G. Mihai, D. Marty, V. A. Guzenko, C. Wild and A. Weber (PSI), who provided technical support; Prof. M. Poggio at the University of Basel for PhD supervision.

## Conflicts of interest

The authors have no conflicts of interest to declare.

## Conflicts of interest

The data that support the findings of this study are available from the corresponding author upon reasonable request.

## References

- [1] Lucia Romano. Etching: The art of semiconductor micromachining. *Micromachines*, 16(2):213, 2025.
- [2] R. P. Srivastava and D. Y. Khang. Structuring of si into multiple scales by metal-assisted chemical etching. *Advanced Materials*, 33(47):e2005932, 2021.
- [3] Chenliang Huo, Jiang Wang, Haoxin Fu, Xian-lun Li, Yi Yang, Hui Wang, Abdul Mateen, Ghulam Farid, and Kui-Qing Peng. Metal-assisted chemical etching of silicon in oxidizing hf solutions: Origin, mechanism, development, and black silicon solar cell application. *Advanced Functional Materials*, 30(52):2005744, 2020.
- [4] Hee Han, Zhipeng Huang, and Woo Lee. Metal-assisted chemical etching of silicon and nanotechnology applications. *Nano Today*, 9(3):271–304, 2014.
- [5] Hailiang Li, Tianchun Ye, Lina Shi, and Changqing Xie. Fabrication of ultra-high aspect ratio (>160:1) silicon nanostructures by using au metal assisted chemical etching. *Journal of Micromechanics and Microengineering*, 27(12):124002, 2017.
- [6] Chieh Chang and Anne Sakdinawat. Ultra-high aspect ratio high-resolution nanofabrication for hard x-ray diffractive optics. *Nature Communications*, 5(1):4243, 2014.
- [7] Xiuling Li. Metal assisted chemical etching for high aspect ratio nanostructures: A review of

characteristics and applications in photovoltaics. *Current Opinion in Solid State and Materials Science*, 16(2):71–81, 2012.

[8] Abdul Mateen, Abdul Jabbar Khan, Zidong Zhou, Altaf Mujear, Ghulam Farid, Wei Yan, Haojie Li, Jiawen Li, and Zhihao Bao. Silicon nanowires via metal-assisted chemical etching for energy storage applications. *ChemSusChem*, 18(2):e202400777, 2024.

[9] Chihoon Kim, Heejo Ahn, and Taeksoo Ji. Flexible pressure sensors based on silicon nanowire array built by metal-assisted chemical etching. *IEEE Electron Device Letters*, 41(8):1233–1236, 2020.

[10] Roey Elnathan, Maria Grazia Barbato, Xiangfu Guo, Anna Mariano, Zixun Wang, Francesca Santoro, Peng Shi, Nicolas H. Voelcker, Xi Xie, Jennifer L. Young, Yunlong Zhao, Wenting Zhao, and Ciro Chiappini. Biointerface design for vertical nanoprobes. *Nature Reviews Materials*, 7:953–973, 2022.

[11] Bo Liu, Amin Farhadi, Theresa Bartschmid, Yamin Zhang, Chunsheng Guo, Shiwei Feng, and Gilles R. Bourret. Nanoscale silicon fingerprints for counterfeit prevention in microchips. *Small*, 21(10):2500878, 2025.

[12] Liyi Li, Guoping Zhang, and Ching-Ping Wong. Formation of through silicon vias for silicon interposer in wafer level by metal-assisted chemical etching. *IEEE Transactions on Components, Packaging and Manufacturing Technology*, 5(8):1039–1049, 2015.

[13] Lucia Romano, Matias Kagias, Joan Vila-Comamala, Konstantins Jefimovs, Li-Ting Tseng, Vitaliy A. Guzenko, and Marco Stampaconi. Metal assisted chemical etching of silicon in the gas phase: a nanofabrication platform for x-ray optics. *Nanoscale Horizons*, 5(5):869–879, 2020.

[14] Liyi Li, Cheng Zhang, Chia-Chi Tuan, Yun Chen, and C. P. Wong. High-aspect-ratio microstructures with versatile slanting angles on silicon by uniform metal-assisted chemical etching. *Journal of Micromechanics and Microengineering*, 28(5):055006, 2018.

[15] Owen J. Hildreth, Devin Brown, and Ching P. Wong. 3d out-of-plane rotational etching with pinned catalysts in metal-assisted chemical etching of silicon. *Advanced Functional Materials*, 21(16):3119–3128, 2011.

[16] S. Hwang, W. Lee, W. N. Carr, and Y. K. Yoon. Metal-assisted chemical etching toward scallop-free-sidewall through-silicon vias: A review. *IEEE Transactions on Components, Packaging and Manufacturing Technology*, 13(11):1848–1860, 2023.

[17] Sami Znati, Juwon Wharwood, Kyle G. Tezanos, Xiuling Li, and Parsian K. Mohseni. Metal-assisted chemical etching beyond si: applications to iii–v compounds and wide-bandgap semiconductors. *Nanoscale*, 16(23):10901–10946, 2024.

[18] Y. Hu, K. Q. Peng, Z. Qiao, X. Huang, F. Q. Zhang, R. N. Sun, X. M. Meng, and S. T. Lee. Metal-catalyzed electroless etching of silicon in aerated hf/h<sub>2</sub>o vapor for facile fabrication of silicon nanostructures. *Nano Lett*, 14(8):4212–9, 2014.

[19] Akhila Mallavarapu, Paras Ajay, and S. V. Sreenivasan. Enabling ultrahigh-aspect-ratio silicon nanowires using precise experiments for detecting the onset of collapse. *Nano Letters*, 20(11):7896–7905, 2020.

[20] X. Li and P. W. Bohn. Metal-assisted chemical etching in hf/h<sub>2</sub>o<sub>2</sub> produces porous silicon. *Applied Physics Letters*, 77(16):2572–2574, 2000.

[21] Hyein Cho, Yejin Han, Geonhwi Kim, Jihwan Jeong, Seongmin Lee, Yebin Ahn, Sang Beom Hong, Soohyeok Park, Inkyeong Park, So Eun Jang, Duck Hyun Youn, and Han-Don Um. Ultrafast room-temperature nanofabrication via ozone-based gas-phase metal-assisted chemical etching for high-performance silicon photodetectors. *Advanced Functional Materials*, n/a(n/a):2502010, 2025.

[22] R. A. Lai, T. M. Hymel, V. K. Narasimhan, and Y. Cui. Schottky barrier catalysis mechanism in metal-assisted chemical etching of silicon. *Ac<sub>s</sub> Applied Materials & Interfaces*, 8(14):8875–8879, 2016.

[23] Zhiwei Xiang, Wei Li, Feng Liu, Feng Tan, Fuxu Han, Xinzhen Wang, Changwei Shao, Mingli Xu, Weiping Liu, and Xikun Yang. Catalyst with a low load of platinum and high activity for oxygen reduction derived from strong adsorption of pt-n<sub>4</sub> moieties on a carbon surface. *Electrochemistry Communications*, 127:107039, 2021.

[24] V. S. Tumashev and V. A. Seleznev. A new technique of au nanopattern formation for metal-assisted chemical etching of silicon. In 2021

*IEEE 22nd International Conference of Young Professionals in Electron Devices and Materials (EDM)*, pages 91–94, 2021.

[25] Owen J. Hildreth, Andrei G. Fedorov, and Ching Ping Wong. 3d spirals with controlled chirality fabricated using metal-assisted chemical etching of silicon. *ACS Nano*, 6(11):10004–10012, 2012.

[26] Lukas L. Janavicius, Julian A. Michaels, Clarence Chan, Dane J. Sievers, and Xiuling Li. Programmable vapor-phase metal-assisted chemical etching for versatile high-aspect ratio silicon nanomanufacturing. *Applied Physics Reviews*, 10(1):011409, 02 2023.

[27] Owen J. Hildreth and Daniel R. Schmidt. Vapor phase metal-assisted chemical etching of silicon. *Advanced Functional Materials*, 24(24):3827–3833, 2014.

[28] Owen J. Hildreth and Daniel R. Schmidt. Vapor phase metal-assisted chemical etching of silicon. *Advanced Functional Materials*, 24(24):3827–3833, 2014.

[29] Zhitian Shi, Konstantins Jefimovs, Marco Stampaconi, and Lucia Romano. High aspect ratio arrays of si nano-pillars using displacement talbot lithography and gas-macetch. *Materials Science in Semiconductor Processing*, 157:107311, 2023.

[30] Raul M. Lema Galindo, Paras Ajay, and S. V. Sreenivasan. Simultaneous micro- and nanoscale silicon fabrication by metal-assisted chemical etch. *Journal of Micro and Nano-Manufacturing*, 10(3):031001, 04 2023.

[31] Hanna Ohlin, Thomas Frisk, and Ulrich Vogt. Single layer lift-off of csar62 for dense nanostructured patterns. *Micromachines*, 14(4):766, 2023.

[32] Hanna Ohlin, Bryan Benz, Lucia Romano, and Ulrich Vogt. Lift-off free catalyst for metal assisted chemical etching of nanostructured silicon zone plates in vapour phase. *Nano Express*, 6(1):015019, 2025.

[33] René H J Vervuurt, Akhil Sharma, Yuqing Jiao, Wilhelmus (Erwin) M M Kessels, and Ageeth A Bol. Area-selective atomic layer deposition of platinum using photosensitive polyimide. *Nanotechnology*, 27(40):405302, 2016.

[34] H. N. Al-Shareef, D. Dimos, B. A. Tuttle, and M. V. Raymond. Metallization schemes for dielectric thin film capacitors. *Journal of Materials Research*, 12(2):347–354, 1997.

[35] Bruno P. Azeredo, Yu-Wei Lin, Arik Avagyan, Mayandi Sivaguru, Keng Hsu, and Placid Ferreira. Direct imprinting of porous silicon via metal-assisted chemical etching. *Advanced Functional Materials*, 26(17):2929–2939, 2016.

[36] Liyi Li, Bo Li, Chuchu Zhang, Chia-Chi Tuan, Zhiqun Lin, and Ching-Ping Wong. A facile and low-cost route to high-aspect-ratio microstructures on silicon via a judicious combination of flow-enabled self-assembly and metal-assisted chemical etching. *Journal of Materials Chemistry C*, 4(38):8953–8961, 2016.

[37] Konrad Rykaczewski, Owen J. Hildreth, Dhaval Kulkarni, Matthew R. Henry, Song-Kil Kim, Ching Ping Wong, Vladimir V. Tsukruk, and Andrei G. Fedorov. Maskless and resist-free rapid prototyping of three-dimensional structures through electron beam induced deposition (ebid) of carbon in combination with metal-assisted chemical etching (mace) of silicon. *ACS Applied Materials & Interfaces*, 2(4):969–973, 2010.

[38] Nguyen Van Toan, Masaya Toda, Takumi Hokama, and Takahito Ono. Cantilever with high aspect ratio nanopillars on its top surface for moisture detection in electronic products. *Advanced Engineering Materials*, 19(11):1700203, 2017.

[39] Akhila Mallavarapu, Brian Gawlik, Michelle Grigas, Mariana Castañeda, Ovadia Abed, Michael P.C. Watts, and S. V. Sreenivasan. Scalable fabrication and metrology of silicon nanowire arrays made by metal assisted chemical etch. *IEEE Transactions on Nanotechnology*, 20:83–91, 2021.

[40] Mark Hrdy, Akhila Mallavarapu, Mariana Castañeda, Paras Ajay, and S. V. Sreenivasan. Scalable au metal-assisted chemical etch nanopatterning using enhanced metal break techniques. *Journal of Micro and Nano-Manufacturing*, 11(1), 2024.

[41] Ayumu Matsumoto, Rin Nishinaka, Yuki Shimada, Kyohei Furukawa, Kyohei Azuma, and Shinji Yae. Metal-assisted etching of n-type and p-type silicon using patterned platinum films: Spatial distribution of mesoporous layer and open circuit potential of silicon. *Journal of The Electrochemical Society*, 170(5):052505, may 2023.

[42] Wataru Kubota, Ryoya Yamaoka, Toru Utsunomiya, Takashi Ichii, and Hiroyuki Sugimura. Vapor-phase chemical etching of silicon assisted by graphene oxide for microfabrication and microcontact printing. *ACS Applied Nano Materials*, 5(8):11707–11714, 2022.

[43] Qingyuan Mao, Jingyuan Zhu, and Zhanshan Wang. Quantitative evaluation of residual resist in electron beam lithography based on scanning electron microscopy imaging and thresholding segmentation algorithm. *Nanotechnology*, 36(4):045301, nov 2024.

[44] L. Romano and M. Stampaoni. Microfabrication of x-ray optics by metal assisted chemical etching: A review. *Micromachines (Basel)*, 11(6):589, 2020.

[45] Lingyu Kong, Binayak Dasgupta, Yi Ren, Parisan K. Mohseni, Minghui Hong, Xiuling Li, Wai Kin Chim, and Sing Yang Chiam. Evidences for redox reaction driven charge transfer and mass transport in metal-assisted chemical etching of silicon. *Scientific Reports*, 6(1):36582, 2016.

[46] Winston Chern, Keng Hsu, Ik Su Chun, Bruno P. de Azeredo, Numair Ahmed, Kyou-Hyun Kim, Jian-min Zuo, Nick Fang, Placid Ferreira, and Xiuling Li. Nonlithographic patterning and metal-assisted chemical etching for manufacturing of tunable light-emitting silicon nanowire arrays. *Nano Letters*, 10(5):1582–1588, 2010.

[47] Nadine Geyer, Bodo Fuhrmann, Zhipeng Huang, Johannes de Boor, Hartmut S. Leipner, and Peter Werner. Model for the mass transport during metal-assisted chemical etching with contiguous metal films as catalysts. *The Journal of Physical Chemistry C*, 116(24):13446–13451, 2012.

[48] Jinquan Huang, Sing Yang Chiam, Hui Huang Tan, Shijie Wang, and Wai Kin Chim. Fabrication of silicon nanowires with precise diameter control using metal nanodot arrays as a hard mask blocking material in chemical etching. *Chemistry of Materials*, 22(13):4111–4116, 2010.

[49] Heini Saloniemi and Mikko Tuohiniemi. Study on  $\text{al}_2\text{o}_3$  film in anhydrous hf vapor. *Solid State Phenomena*, 187:45–48, 04 2012.

[50] K.R. Williams, K. Gupta, and M. Wasilik. Etch rates for micromachining processing-part ii. *Journal of Microelectromechanical Systems*, 12(6):761–778, 2003.

[51] Kurt R. Mikeska and Stephen J. Bennison. Corrosion of alumina in aqueous hydrofluoric acid. *Journal of the American Ceramic Society*, 82(12):3561–3566, 1999.

[52] Thor Bakke, Jan Schmidt, Martin Friedrichs, and Benjamin Völker. Etch stop materials for release by vapor hf etching. In *Proc. Micromech. Eur. Workshop*, volume 16, pages 103–106, 2005.

[53] Fukuta Yamato, Fujita Hiroyuki, and Toshiyoshi Hiroshi. Vapor hydrofluoric acid sacrificial release technique for micro electro mechanical systems using labware. *Japanese Journal of Applied Physics*, 42(6R):3690, 2003.

[54] Jungkil Kim, Hee Han, Young Heon Kim, Suk-Ho Choi, Jae-Cheon Kim, and Woo Lee. Au/ag bilayered metal mesh as a si etching catalyst for controlled fabrication of si nanowires. *ACS Nano*, 5(4):3222–3229, 2011.

[55] C. Hedlund, H. O. Blom, and S. Berg. Microloading effect in reactive ion etching. *Journal of Vacuum Science & Technology A: Vacuum, Surfaces, and Films*, 12(4):1962–1965, 1994.

[56] Yun Chen, Cheng Zhang, Liyi Li, Chia-Chi Tuan, Fan Wu, Xin Chen, Jian Gao, Yong Ding, and Ching-Ping Wong. Fabricating and controlling silicon zigzag nanowires by diffusion-controlled metal-assisted chemical etching method. *Nano Letters*, 17(7):4304–4310, 2017.

[57] David A Czaplewski, Martin V Holt, and Leonidas E Ocola. The range and intensity of backscattered electrons for use in the creation of high fidelity electron beam lithography patterns. *Nanotechnology*, 24(30):305302, 2013.

[58] M. Albrechtsen, B. Vosoughi Lahijani, R. E. Christiansen, V. T. H. Nguyen, L. N. Casses, S. E. Hansen, N. Stenger, O. Sigmund, H. Jansen, J. Mork, and S. Stobbe. Nanometer-scale photon confinement in topology-optimized dielectric cavities. *Nat Commun*, 13(1):6281, 2022.

[59] Kenan Li, Michael J. Wojcik, Ralu Divan, Leonidas E. Ocola, Bing Shi, Daniel Rosenmann, and Chris Jacobsen. Fabrication of hard x-ray zone plates with high aspect ratio using metal-assisted chemical etching. *Journal of Vacuum Science & Technology B*, 35(6):06G901, 2017.

[60] Michał Rawlik, Alexandre Pereira, Simon Spindler, Zhentian Wang, Lucia Romano, Konstantins Jefimovs, Zhitian Shi, Maxim Polikarpov, Jinqiu Xu, Marie-Christine Zdora, Stefano van Gogh, Martin Stauber, Eduardo G. Yukihara, Jeppe B. Christensen, Rahel A. Kubik-Huch, Tilo Niemann, Cornelia Leo, Zsuzsanna Varga, Andreas Boss, and Marco Stampanoni. Increased dose efficiency of breast ct with grating interferometry. *Optica*, 10(7):938–943, Jul 2023.

[61] Kirsten Taphorn, Fabio De Marco, Jana Andrejewski, Thorsten Sellerer, Franz Pfeiffer, and Julia Herzen. Grating-based spectral x-ray dark-field imaging for correlation with structural size measures. *Scientific Reports*, 10(1), 2020.

[62] J. Vila-Comamala, K. Jefimovs, J. Raabe, B. Kaulich, and C. David. Silicon fresnel zone plates for high heat load x-ray microscopy. *Microelectronic Engineering*, 85(5-6):1241–1244, 2008.

[63] Jisoo Kim, Matias Kagias, Federica Marone, and Marco Stampanoni. X-ray scattering tensor tomography with circular gratings. *Applied Physics Letters*, 116(13):134102, 2020.

[64] Kaye S. Morgan, Peter Modregger, Sarah C. Irvine, Simon Rutishauser, Vitaliy A. Guzenko, Marco Stampanoni, and Christian David. A sensitive x-ray phase contrast technique for rapid imaging using a single phase grid analyzer. *Opt. Lett.*, 38(22):4605–4608, Nov 2013.

[65] S. Spindler, M. Rawlik, L. Romano, A. Pereira, P. Guo, Z. Wang, and M. Stampanoni. Simulation study of an x-ray diffraction beamlet array for dark-field chest ct. *Opt Express*, 33(11):23835–23849, 2025.

[66] Zhitian Shi, Konstantins Jefimovs, Joan Vila-Comamala, Alexandre Pereira, Daniel Josell, Marco Stampanoni, and Lucia Romano. Deep-reactive-ion-etching in x-ray grating fabrication: a review. *Materials Science in Semiconductor Processing*, 201, 2026.

[67] Angela M. Baracu, Christopher A. Dirdal, Andrei M. Avram, Adrian Dinescu, Raluca Muller, Geir Uri Jensen, Paul Conrad Vaagen Thrane, and Hallvard Angelskår. Metasurface fabrication by cryogenic and bosch deep reactive ion etching. *Micromachines*, 12(5):501, 2021.

[68] L. Y. Kong, Y. S. Zhao, B. Dasgupta, K. Hippalgaonkar, X. L. Li, W. K. Chim, and S. Y. Chim. Minimizing isolate catalyst motion in metal-assisted chemical etching for deep trenching of silicon nanohole array. *Acs Applied Materials & Interfaces*, 9(24):20981–20990, 2017.